Available online at www.sciencedirect.com

ScienceDirect

Advances in Space Research 61 (2018) 823–829

ADVANCES IN SPACE RESEARCH (a COSPAR publication)

www.elsevier.com/locate/asr

VLBI observations to the APOD satellite

Jing Sun [a,b,*], Geshi Tang [a], Fengchun Shu [c], Xie Li [a], Shushi Liu [a], Jianfeng Cao [a], Andreas Hellerschmied [d], Johannes Böhm [d], Lucia McCallum [e], Jamie McCallum [e], Jim Lovell [e], Rüdiger Haas [f], Alexander Neidhardt [g], Weitao Lu [a], Songtao Han [a], Tianpeng Ren [a], Lue Chen [a], Mei Wang [a], Jinsong Ping [h]

[a] *Beijing Aerospace Control Center, 26 Beiqing Road, Beijing 100094, China*
[b] *Xinjiang Astronomical Observatory, 150 Science 1-Street, Urumqi 830011, China*
[c] *Shanghai Astronomical Observatory, 80 Nandan Road, Shanghai 200030, China*
[d] *Technische Universität Wien, Gußhausstraße 27-29, 1040 Vienna, Austria*
[e] *University of Tasmania, Private Bag 37, 7001 Hobart, Australia*
[f] *Chalmers University of Technology, Onsala Space Observatory, 43992 Onsala, Sweden*
[g] *Technische Universität München, Geodetic Observatory Wettzell, Germany*
[h] *National Astronomical Observatory, 20A Datun Road, Beijing 100012, China*

Received 3 May 2017; received in revised form 20 October 2017; accepted 28 October 2017
Available online 6 November 2017

Abstract

The APOD (Atmospheric density detection and Precise Orbit Determination) is the first LEO (Low Earth Orbit) satellite in orbit co-located with a dual-frequency GNSS (GPS/BD) receiver, an SLR reflector, and a VLBI X/S dual band beacon. From the overlap statistics between consecutive solution arcs and the independent validation by SLR measurements, the orbit position deviation was below 10 cm before the on-board GNSS receiver got partially operational. In this paper, the focus is on the VLBI observations to the LEO satellite from multiple geodetic VLBI radio telescopes, since this is the first implementation of a dedicated VLBI transmitter in low Earth orbit. The practical problems of tracking a fast moving spacecraft with current VLBI ground infrastructure were solved and strong interferometric fringes were obtained by cross-correlation of APOD carrier and DOR (Differential One-way Ranging) signals. The precision in X-band time delay derived from 0.1 s integration time of the correlator output is on the level of 0.1 ns. The APOD observations demonstrate encouraging prospects of co-location of multiple space geodetic techniques in space, as a first prototype.

Keywords: APOD; VLBI; GNSS; SLR; Space ties

1. Introduction

The VLBI technique has been used successfully and extensively for tracking a number of deep-space missions since the second half of the 1980s. Another application of VLBI is to track Earth orbiting satellites, like the highly elliptical orbit satellite TanCe-1, Earth synchronous orbit satellites (80°E and 140°E) (Shu et al., 2003), and GNSS ones (Tornatore et al., 2014; Plank et al., 2015a, 2017). The APOD (Atmospheric density detection and Precise Orbit Determination) is the first LEO (Low Earth Orbit) satellite that was observed with GNSS, SLR, and VLBI. Observing the APOD satellite is challenging since the mutual visibility depends on the altitude of the satellite and the separation of the radio telescopes (Hase, 1999). The APOD satellite travels through the horizon to horizon

* Corresponding author at: Beijing Aerospace Control Center, 26 Beiqing Road, Beijing 100094, China.
E-mail address: sunjing@shao.ac.cn (J. Sun).

https://doi.org/10.1016/j.asr.2017.10.046
0273-1177/

on the observing stations for tens of seconds, and there are only 2–3 passages through the zone of mutual visibility per day. Observations to the APOD satellite are promising in the area of space ties, combining all techniques by the installation of adequate technique-specific sensors on a single satellite platform, e.g. with the proposed GRASP mission (Geodetic Reference Antenna in Space) (Bar-Sever et al., 2011) or the European E-GRASP/Eratosthenes mission (Biancale, 2016).

We will describe the APOD mission and GNSS/SLR observations in Section 2. In Section 3 the VLBI observations to the APOD satellite and data processing are investigated, in particular focusing on the VLBI observations with geodetic VLBI radio telescopes. The designed cross-correlation algorithms for this LEO satellite and preliminary results are provided in Section 4, considering the low accuracy of the APOD orbit. Finally in Section 5, discussions on present results and further developments are presented.

2. APOD mission

2.1. General descriptions

On Sept. 20, 2015, 20 satellites were launched successfully by a Chinese CZ-6 rocket from TaiYuan Satellite Launch Center, and then operated in a circular, near-polar orbit with an altitude of 520 km. Among these satellites, a set of four CubSats, named APOD, are projected for measurement of atmospheric density by in situ sensors and by analyzing the orbit evolution (Tang et al., 2016). The precise orbit prediction for LEO spacecraft is very important for space debris collision avoidance (Liou, 2006), orbit manoeuvres of LEO spacecraft, as well as rendezvous and docking at space stations. The major challenge for accurate orbit prediction of LEO satellites is inaccuracy of atmospheric density model at high altitudes. Improving the accuracy of atmospheric density models needs high quality observations of mass density (direct or indirect) with sufficient spatial and temporal resolutions and coverage. From the 1960s, many techniques have been developed to measure high altitudes atmospheric mass density and composition, including drag-derived means by orbit of spacecraft, in situ measurement by neutral mass spectrometers, ultraviolet remote sensing and other techniques by rockets payload or from ground base (Emmert, 2015). Still, more extensive spatial and temporary coverage would be needed to improve the accuracy of atmospheric density models because of the complex variation of atmosphere. And the cost to meet this requirement is huge. But the development of low cost CubSats provides a very good opportunity to detect atmospheric density in a more extensive spatial coverage. Thus BACC/AFDL (Beijing Aerospace Control Center/Aerospace Flight Dynamic Laboratory) proposed the APOD project to study the technology of in situ detection by payload instruments and derivation by precise orbits. The APOD satellites were manufactured by DFH Co., the ground segment is controlled by BACC/AFDL including payload operation as well as science data receiving, processing, archiving and distribution. The APOD mission aims to detect atmospheric density below 520 km.

The APOD family includes a nano satellite (named APOD-A) and three pico satellites (named APOD-B, APOD-C, APOD-D). All four satellites are flying in a circular, near polar-orbit with an inclination at about 97 degrees and all four satellites were located at 520 km altitude after being launched. Then APOD-A was descended to a 470 km altitude orbit two weeks later. In order to obtain atmospheric density by an in situ detector and by deriving density from precise orbits, payloads used for precise orbit determination and density detection are mounted on the APOD-A satellite (see Fig. 1), which include the atmospheric density detector, a dual-frequency GNSS (GPS/BD) receiver, an SLR reflector and a VLBI X/S dual band beacon. The payloads of multiple observations on the APOD-A satellite are listed in Table 1. The mass of APOD-A is 25.88 kg and its size is 391 mm × 398 mm × 398 mm. It should be mentioned that it takes great efforts to integrate these instruments in such a miniature satellite. APOD-A is a three-axis stabilized satellite, and its attitude stability is maintained by gyros, magnetometer, and sun sensor. The in-orbit commissioning of the platform and payloads was finished in December 2015 and APOD has been in ordinary operation since then. The satellite guaranteed lifetime is 12 months, but the APOD satellites are still working as of September 2017, except that the GNSS receiver is not providing pseudorange and carrier phase raw data any more.

2.2. GNSS observations

The POD (Precise Orbit Determination) is performed by GPS L1/L2 double differences carrier phase data and pseudorange data. BACC/AFDL generates precise orbit solution using its own proprietary software. The geophysical models and estimated parameters are summarized in Table 2. The orbit has been verified by the XiAn Satellite Control Center (XSCC) using the Bernese software (Dach et al., 2015) (personal communications with Jun Zhu). To evaluate orbit precision, we produced orbit overlaps by comparing the differences of two consecutive orbit solutions (arcs) spanning 10 h and computed independently. We evaluated the RMS (Root Mean Square) differences for the radial, along-track and cross-track components during arc common time period. The averaged RMS are 5, 7, and 3 cm for these three components of the overlap respectively. The left plot in Fig. 2 depicts the post-fit residuals of the GPS L1/L2 POD solution of APOD-A. The RMS of pseudorange residuals and carrier phase residuals are 1.95 m and 1.58 cm, respectively.

On Jan. 21, 2016, the GNSS receiver on APOD-A partially ceased functioning. There are no carrier phase and pseudorange raw data recorded from that time on, only

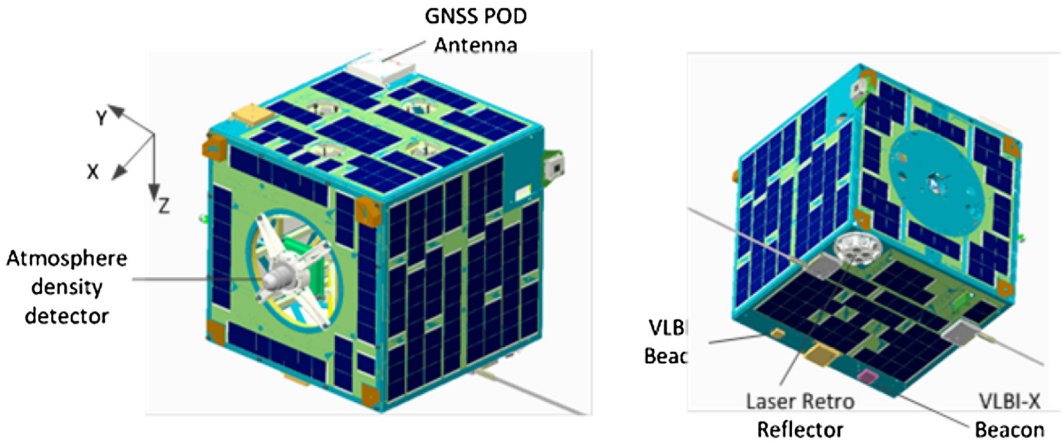

Fig. 1. Physical layout of the APOD-A nano satellite with the location of scientific instruments (Left: Front side view; Right: Bottom side view).

Table 1
APOD-A nano satellite payloads.

GNSS Receiver	Mode	GPS/BDS
	GPS Frequency/MHz	L1:1575.42, L2:1227.60
	BDS Frequency/MHz	B1:1561.098, B3:1250.618
	Sampling Rate/s	8
Laser Retro Reflector	Type	Pyramid
	Number of cube corner prisms	9
VLBI Beacon	S-Band Frequency/MHz	$f_{S_{carrier}} = 2262$ $f_{S_{dor1}} = 2256.86$ $f_{S_{dor2}} = 2260.97$ $f_{S_{dor3}} = 2263.03$ $f_{S_{dor4}} = 2267.14$
	X-Band Frequency/MHz	$f_{X_{carrier}} = 8424$ $f_{X_{dor1}} = 8404.85$ $f_{X_{dor2}} = 8420.17$ $f_{X_{dor3}} = 8427.83$ $f_{X_{dor4}} = 8443.15$

coordinates of the APOD-A satellite determined on-board are available. There are four sets of orbit data transmitted every day when the satellite passes the tracking stations. The orbit determination residuals are 10–20 m, as shown in the right plot of Fig. 2.

2.3. SLR observations

The International Laser Ranging Service (ILRS) (Pearlman et al., 2002) provides SLR (Satellite Laser Ranging) measurements to the APOD satellites. BACC/AFDL is responsible for guiding the SLR station by uploading satellite prediction files in Consolidated Prediction Format (CPF) to the ILRS website. APOD-A nano satellite is regularly tracked by 13 globally distributed SLR stations since 02 October 2015 and the observations are continuing. More than 4000 normal points have been determined until now. The names of APOD satellites in the ILRS are PN-1A, -1B, -1C, -1D, respectively. The measurement conditions for the APOD-A nano satellite within the ILRS website are described in Table 3. The SLR measurements are used for an independent validation of the GPS-derived orbits. ITRF2008 coordinates are used for the SLR stations, the center of mass (CoM) offset of the LRR array is corrected according to the parameter described at the ILRS website. The normal point data with O-C larger than 30 cm and elevation angles less than 15 deg are removed. Fig. 3 depicts the differences between the SLR measurement ranges and the ranges derived by GPS L1/L2 carrier phase POD, the tie between SLR reflector and GNSS receiver on the satellite-fixed reference system has been corrected. From the overlap statistics between consecutive solution arcs and the independent validation by SLR measurements, the mean value and standard deviation for all stations are −2.93 cm and 9.85 cm before the on-board GNSS receiver got partially operational. More SLR data obtained in the future would be used to improve the orbit determination of APOD.

Table 2
Geophysical models and estimation parameters.

Geophysical models	
Gravity/Tides	JGM3 (Tapley et al., 1996)/IERS 2010
Atmospheric density	MSIS-00 (Picone et al., 2002)
Earth orientation	IERS final2000
Planetary ephemeris	DE421
Data weighting	GPS pseudorange 1 m GPS phase 1 cm
Estimation parameters	
Measurement model	Carrier phase ambiguity per pass
Force model	State (position and velocity) Cd (coefficient of atmospheric drag) per 1.5 h 1-cpr (cycle per revolution) accelerations per 1.5 h
Arc length	1-day arcs

3. VLBI observations and data processing

APOD is the first LEO satellite with a VLBI S/X beacon in space, and its DOR (Differential One-way Ranging) tone frequencies are designed in accordance with CCSDS (Con-

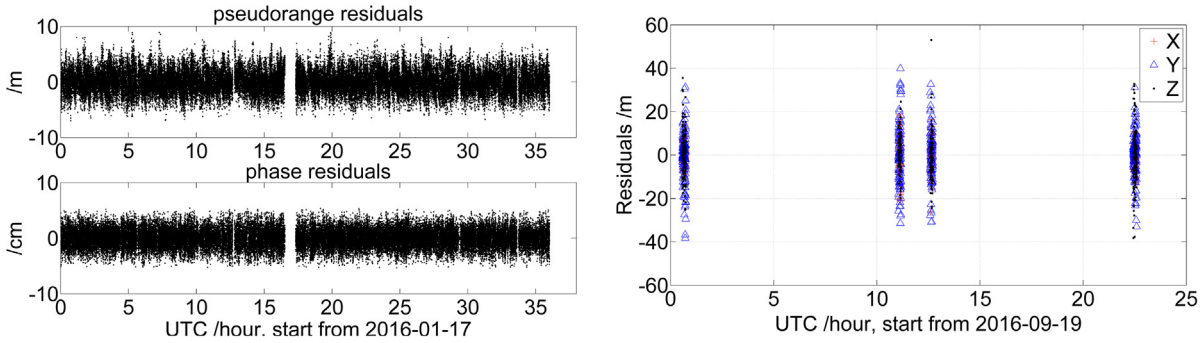

Fig. 2. Orbit determination residuals. Left plot: residuals in POD of GPS pseudorange and carrier phase data before the failure of the on-board GNSS receiver. The RMS of pseudorange residuals and carrier phase residuals are 1.95 m and 1.58 cm, respectively. Right plot: residuals of coordinate data after the failure of the onboard GNSS receiver. The coordinate residuals are about 10–20 m.

Table 3
APOD-A nano satellite mission parameters.

Satellite Name	PN-1A
Satellite (COSPAR) ID	1504905
SIC Code	2203
Satellite Catalog (NORAD) Number	40903
NP Indicator	1
Bin Size (Seconds)	5

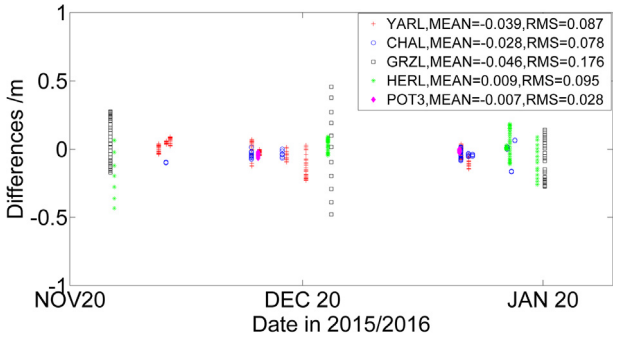

Fig. 3. Differences between the SLR measurement ranges and the ranges derived by GPS L1/L2 carrier phase POD. The mean value and standard deviation of each station are marked in the figure. Their values for all stations are −2.93 cm and 9.85 cm, respectively.

sultative Committee for Space Data Systems) recommendations (CCSDS 401.0-B) (CCSDS 401.0-B, 1994). The satellite EIRP (Effective Isotropic Radiated Power) is 4 dBm, and the strength of DOR tone signal is 12 dB weaker than the carrier signal. The transmitted signal from VLBI beacon is circular polarized. The on-board quartz is used to generate the frequency with an accuracy of $\pm 1 \times 10^{-6}$ and a frequency stability of 1×10^{-9}. We use VLBI antennas in geodetic mode to observe signals emitted by the APOD-A satellite. Several preparatory tests were required for obtaining good data that could be processed. The first VLBI observations to APOD were carried out successfully with three AuScope (Lovell et al., 2013; Plank et al., 2015b) VLBI observatories on April 4, 2016. Since then, a series of VLBI observations has been carried out. The participating VLBI radio telescopes of the IVS (International VLBI Service for Geodesy and Astrometry) (Schuh and Behrend, 2012) members are shown in Fig. 4. The network observing stations were selected considering geometry and slewing speed constraints. Table 4 lists the APOD observations by VLBI radio telescopes. It should also be mentioned that the APOD is not continuously sending tones in X- and S-band, so the mission controller has to turn the transmitter on before each session and turn it off after the observation. The schedules were generated with the Vienna VLBI Software VieVS (Böhm et al., 2012), considering slew speed limitations, cable wrap limits, antenna axis limits, horizon masks and a minimum sun-distance (Sun et al., 2014; Hellerschmied et al., 2014, 2015, 2016). It required a lot of efforts to adapt antenna control software for tracking fast LEO satellites. It is also shown in Table 4 that several modes have been implemented for tracking APOD. During intensive APOD tracking in November 2016 (Session 316a to 332a) carried out by the Australian AuScope antennas, this tracking mode uses a list of time-tagged Az/El positions as input. The advantage of this scheme is that such a list is processed directly by the antenna motion controller by interpolation between the nodes of the tracking table. The APOD carrier and DOR signals of X/S dual band were recorded. From Session 095a to 263c, individual channels were set for each tone, while several DOR tones were recorded within one 16 MHz channel from Session 316a to 332a.

The VLBI raw data were transferred to BACC/AFDL for further processing and cross-correlating. In order to handle the raw data received from APOD or other near-field targets, we have developed a software tool for correlator model calculation and data correlation. The correlator model delay was calculated as a sum of geometric delay and station clock offset, and expressed as a 5th-order polynomial for each scan. A scan means the time period during which a network of stations observes the same source simultaneously. The APOD positions for these calculations were based on final ephemerides with one second temporal resolution. Our data correlation algorithm implements the FX correlator architecture described in full detail by Thompson (Thompson, 1999). Briefly the algorithm does

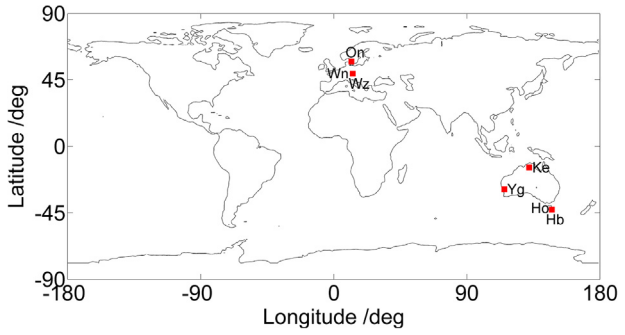

Fig. 4. Distribution of VLBI radio telescopes participating in APOD observations.

the following: data streams from each station are aligned with integer-bit delay, phase corrected by fringe rotation, converted into frequency domain with a Fast Fourier Transform (FFT) and corrected for fractional-bit error. The resulting complex data are then cross multiplied for each baseline and accumulated over a certain period called integration time. The final correlator output is the time series of auto and cross-spectrum for each IF (Intermediate Frequency) band and each baseline.

4. Preliminary results

In this paper, we would like to show the new observations of a LEO spacecraft by VLBI using session 318c as an example, because of the same setting for all the intensive APOD tracking in November 2016. The correlation and data analyses for all the VLBI experiments with AuScope VLBI array are in preparation for future paper to show the orbit improvement and differences of multiple space geodetic observations (personal communications with Andreas Hellerschmied). The session 318c was observed at a 1 Gbps data rate with 16 IF channels of 16 MHz bandwidth and 2-bit sampling. The first 10 IF channels were spread at X-band and the remaining 6 IF channels were spread at S-band. The X-band DOR tones were recorded in the IF 3, 4 and 5, while the S-band DOR tones were recorded in the IF 14 (as seen in Fig. 5). We attempted to correlate using 1024 FFT points and 1-s integration time, but failed to obtain fringes of the APOD signals due to large uncertainties in the correlator model which was calculated by using the APOD ephemerides with low accuracy. Thus we developed a step-wise approach to obtain good fringes and accurate delay estimates.

Step 1. Search for coarse delay rate. We fetched 1-s data from a scan, and performed the data correlation by using 1-ms integration time. Such short integration time allows us to search fringe rate in the range of $[-500, 500]$ Hz, equivalent to the delay rate window within $[-227, 227]$ ns/s at sky frequency 2.2 GHz. The interferometric phase of the main carrier over the time was extracted from the correlation output, and modelled by applying a linear fit. Then the coarse delay rate was obtained and used to update the correlator model.

Step 2. Search for fine delay rate. We performed the data correlation of the whole scan by using the updated correlator model and setting the integration time to 0.1 s. Again the interferometric phase of the main carrier over the time was extracted, and modelled by applying a 2nd-order polynomial fit. Then the delay rate and acceleration were obtained and used to update the correlator model.

Step 3. Search for coarse delay. Based on the updated correlator model, we correlated the same data once again using 16384 FFT points, which corresponds to a delay search window within $[-512, 512]$ μs for a 16 MHz-wide channel. We identified the cross spectra of telemetry signals within ±50 kHz of the main carrier on the frequency domain, and performed a linear fit of the phase versus frequency data to obtain the coarse delay. Thus, an accurate correlator model was reconstructed and used for the fine delay search.

Step 4. Production correlation. Similar to the correlation of natural extragalactic radio sources, now we can use accurate correlator model to correlate the whole scan, using 0.1-s integration time and 1024 FFT points. The correlation output was used for fine delay search.

Step 5. Search for fine delay at S-band. The main carrier and DOR tones are all located in one single channel at S-band. Similar to step 3, we performed a linear fit of the

Table 4
List of APOD observations by VLBI radio telescopes.

Session	Stations	Tracking mode	Band width/Quantization
095a	Hb + Ke + Yg	Ra/De input	1 M/1-bit
197c	On	Ra/De input	1 M/2-bit
200a	Ke + Yg	TLE input	2 M/2-bit
202a	Ke + Yg	TLE input	2 M/2-bit
263a/b/c	On + Wn + Wz	Ra/De input (On) TLE input (Wn + Wz)	2 M/2-bit
316a	Ke + Yg	Az/El input	16 M/2-bit
317a/b	Ho + Hb + Ke + Yg	Az/El input	16 M/2-bit
318b/c/d	Ho + Hb + Ke + Yg	Az/El input	16 M/2-bit
319a	Ho + Hb + Ke + Yg	Az/El input	16 M/2-bit
331a	Ho + Hb + Ke + Yg	Az/El input	16 M/2-bit
332a	Ho + Hb + Ke + Yg	Az/El input	16 M/2-bit

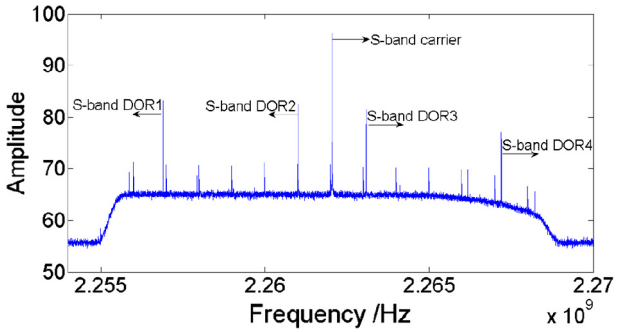

Fig. 5. Auto-correlation of five S-band signals at station Hb in Session 318c, the other tones are phase calibration signals.

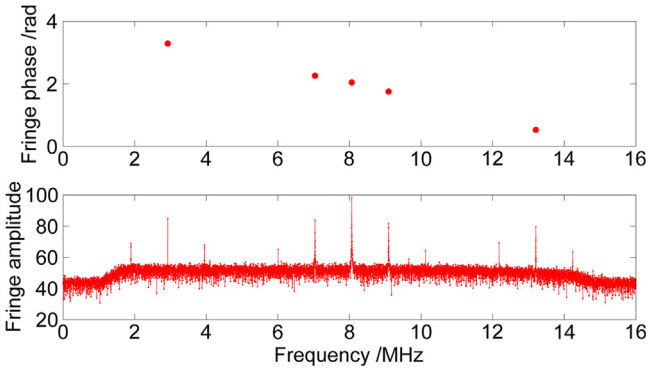

Fig. 6. Cross-correlation fringe of five S-band signals for baseline Hb-Ke in Session 318c, i.e. one carrier and four DOR tones. The linear fit of fringe phase versus frequency is seen.

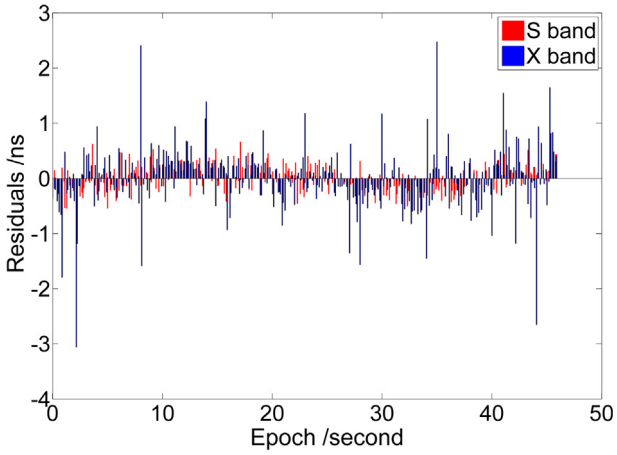

Fig. 7. Residual multiband delays of S/X dual band signals for baseline Hb-Ke in Session 318c, with respect to the computed time delays. The RMS scatter of residuals over 45-s passage for S-band and X-band is 0.22 ns and 0.52 ns, respectively.

phase versus frequency data, but on a wider bandwidth to obtain the fine delay in an interval of 0.1 s. Plots of fringe phases and amplitudes derived from processing the correlator output are shown in Fig. 6. When the time delay from multiband synthesis was received, we aligned the phase offsets of different channels, and performed a linear fit with all DOR tones. The statistic of 0.6 ns is the formal error of multiband delay estimation in average. Fig. 7 shows the residual multiband delays for baseline Hb-Ke, and the RMS scatter of residuals over the 45-s passage for S-band is 0.22 ns.

Step 6. Search for fine delay at X-band. The main carrier and DOR tones are located in three different IF channels at X-band. In order to obtain bandwidth synthesis delay, we aligned the phase offsets of different channels, and performed a linear fit with all DOR tones to obtain the fine delay at X-band. Fig. 7 also depicts the residual multiband delays for baseline Hb-Ke, scattered in X-band most likely due to pointing losses of narrower beamwidth of X-band. The average formal error of multiband delay estimation in time delay derived from the correlator output averaged over 45 s is 0.1 ns. The longer integration time and more accurate phase offsets bear the prospect of further improvements.

Using session 318c as example, the integration time is set to be 0.1 s and the mutual visibility is only 45 s long. So the number of VLBI normal points is 450. Considering the mutual visibility and cut-off elevation, there are three APOD passes per day at most.

5. Discussions

We consider the first results of multi-technique observations of APOD satellite encouraging. The APOD project can be considered as a prototype of an instrument that implements co-location of multiple space geodetic techniques in space. The three-dimension position deviation of the APOD satellite was below 10 cm with validation independently by SLR observations before the failure of the onboard GNSS receiver. We have succeeded to track successfully the LEO satellite with radio telescopes continuously during its several-minutes passage through the mutual visibility zone. Strong fringes were obtained by iterated cross-correlation and the variation of fringe phase over passage is less than 1 rad. With synthesized bandwidth, the precision of time delay derived from the correlator output is 0.6 ns and 0.1 ns, for S-band and X-band respectively. We learned from these observing campaigns that algorithms of antenna control and data analysis which were not originally designed for this type of observations require further substantial improvement. The tracking mode of Az/El input should be implemented for satellite observations. We expect that using longer integration time, the accuracy of phase offset determination will improve. We are going to continue APOD observations as long as it is remained operational. More VLBI delay observations would be used to improve the APOD orbit and analyze the systematic error of multiple space geodetic techniques.

Acknowledgement

This study made use of data collected through the AuScope initiative. AuScope Ltd is funded under the National

Collaborative Research Infrastructure Strategy (NCRIS), an Australian Commonwealth Government Programme. The authors thank the Austrian Science Fund (FWF) for funding projects SORTS I 2204 and J 3699-N29. The authors wish to thank the staff at the stations who participated in this work and many colleagues for their hints and discussions.

References

Bar-Sever, Y., Bertiger, W., Desai, S., Gross, R., Haines, B., Wu, S., Nerem, S., 2011. Geodetic Reference Antenna in Space (GRASP): A Mission to Enhance GNSS and the Terrestrial Reference Frame. <http://www.pnt.gov/advisory/2011/06/bar-sever.pdf>.

Biancale, R., 2016. E-GRASP/Eratosthenes: a satellite mission proposal submitted to the ESA/Earth Explorer-9 call. In: First International Workshop on VLBI Observations of Near-field Targets, Bonn, Germany, October 5–6, 2016. <http://www3.mpifr-bonn.mpg.de/div/meetings/vonft/pdf-files/talks/E-GRASP_Eratosthenes_Biancale>.

Böhm, J., Böhm, S., Nilsson, T., Pany, A., Plank, L., Spicakova, H., Teke, K., Schuh, H., 2012. The new Vienna VLBI Software VieVS. In: Proceedings of the 2009 IAG Symp., Buenos Aires, Argentina, vol. 136, 126, pp. 1007–1011. https://doi.org/10.1007/978-3-642-20338-1.

Consultative Committee for Space Data Systems (CCSDS), 1994. Radio Frequency and Modulation Systems-Part 1: Earth Stations and Spacecraft. CCSDS 401.0-B, Blue Book, Issue 1 & 2 Recs.

Dach, R., Lutz S., Walser P., Fridez P., 2015. Bernese GNSS Software Version 5.2. User manual. Astronomical Institute, University of Bern, Bern Open Publishing. https://doi.org/10.7892/boris.72297. ISBN: 978-3-906813-05-9.

Emmert, J.T., 2015. Thermospheric mass density: a review. Adv. Space Res. 56 (5), 773–824. https://doi.org/10.1016/j.asr.2015.05.038.

Hase, H., 1999. Phase centre determinations at GPS-satellites with VLBI. In: Proceedings of 13th EVGA, pp. 273–277.

Hellerschmied, A., Plank, L., Neidhardt, A., Haas, R., Böhm, J., Plötz, C., Kodet, J., 2014. Observing satellites with VLBI radio telescopes – practical realization at Wettzell. In: Behrend, D., Baver, K., Armstrong, K. (Eds.), IVS 2014 General Meeting Proceedings VGOS: The New VLBI Network. Science Press, pp. 441–445.

Hellerschmied, A., Böhm, J., Neidhardt, A., Kodet, J., Haas, R., Plank, L., 2015. Scheduling VLBI Observations to Satellites with VieVS. In: IAG Symp. Springer, Berlin, Heidelberg, pp. 1–6. https://doi.org/10.1007/1345_2015_183.

Hellerschmied, A., Plank, L., McCallum, J., Sun, J., Böhm, J., 2016. Scheduling of VLBI satellite observations with VieVS. In: First International Workshop on VLBI Observations of Near-field Targets, Bonn, Germany, October 5–6, 2016.

Liou, J.C., 2006. Collision activities in the future orbital debris environment. Adv. Space Res. 38, 2102–2106.

Lovell, J., McCallum, J., Reid, P., McCulloch, P., Baynes, B., Dickey, J., Shabala, S., Watson, C., Titov, O., Ruddick, R., Twilley, R., Reynolds, C., Tingay, S., Shield, P., Adada, R., Ellingsen, S., Morgan, J., Bignall, H., 2013. The AuScope geodetic VLBI array. J. Geod. 87, 527–538.

Pearlman, M.R., Degnan, J.J., Bosworth, J.M., 2002. The international laser ranging service. Adv. Space Res. 30 (2), 135–143. https://doi.org/10.1016/S0273-1177(02)00277-6.

Picone, J.M., Hedin, A.E., Drob, D.P., Aikin, A.C., 2002. NRLMSISE-00 empirical model of the atmosphere: statistical comparisons and scientific issues. J. Geophys. Res. 107 (A12), 1468. https://doi.org/10.1029/2002JA009430.

Plank, L., Böhm, J., Schuh, H., 2015a. Simulated VLBI satellite tracking of the GNSS constellation: observing strategies. In: Rizos, C., Willis, P. (Eds.), IAG 150 Years, IAG Symp, vol. 143. Springer, Cham, pp. 85–90.

Plank, L., Lovell, J., Shabala, S., Böhm, J., Titov, O., 2015b. Challenges for geodetic VLBI in the southern hemisphere. Adv. Space Res. 56 (2), 304–313.

Plank, L., Hellerschmied, A., McCallum, J., Böhm, J., Lovell, J., 2017. VLBI observations of GNSS-satellites: from scheduling to analysis. J. Geod. https://doi.org/10.1007/s00190-016-0992-8.

Schuh, H., Behrend, D., 2012. VLBI: a fascinating technique for geodesy and astrometry. J. Geodyn. 61, 6880. https://doi.org/10.1016/j.jog.2012.07.007.

Shu, F., Zhang, X., Zheng, W., 2003. VLBI observations of geosynchrononous satellites. Ann. Shanghai Observ. Acad. Sin. 24, 105–111.

Sun, J., Böhm, J., Nilsson, T., Krásná, H., Böhm, S., Schuh, H., 2014. New VLBI2010 scheduling strategies and implications on the terrestrial reference frames. J. Geod. 88, 449–461.

Tang, G., Sun, J., Li, X., Liu, S., Chen, G., Ren, T., Wang, G., 2016. APOD mission status and observations by VLBI. In: Dirk, B., Karen, D.B., Kyla, L.A. (Eds.), International VLBI Service for Geodesy and Astrometry 2016 General Meeting Proceedings New Horizons with VGOS, NASA/CP-2016-219016, pp. 363–367.

Tapley, B.D., Watkins, M.M., Ries, J.C., Davis, G.W., Eanes, R.J., Poole, S.R., Rim, H.J., Schutz, B.E., Shum, C.K., Nerem, R.S., Lerch, F.J., Marshall, J.A., Klosko, S.M., Pavlis, N.K., Williamson, R.G., 1996. The joint gravity model 3. J. Geophys. Res. 101 (B12), 28029–28049.

Thompson, A.R., 1999. Synthesis imaging in radio astronomy II. In: Taylor, G.B., Carilli, C.L., Perley, R.A. (Eds.), ASP, San Francisco, pp. 11.

Tornatore, V., Haas, R., Casey, S., Duev, D., Pogrebenko, S., Calvés, G. M., 2014. Direct VLBI observations of global navigation satellite system signals. In: Rizos, C., Willis, P. (Eds.), Earth on the Edge: Science for a Sustainable Planet, IAG Symp, vol. 139. Springer, Berlin, Heidelberg, pp. 247–252.